Relaxivity Optimization of a PEGylated Iron-Oxide-Based Negative Magnetic Resonance Contrast Agent for T_2-Weighted Spin–Echo Imaging

Elmar Pöselt,[†,*] Hauke Kloust,[†] Ulrich Tromsdorf,[†] Marcus Janschel,[†] Christoph Hahn,[†] Christoph Maßlo,[‡] and Horst Weller[†,*]

[†]Institute of Physical Chemistry, University of Hamburg, Grindelallee 117, 20146 Hamburg, Germany, and [‡]Department of Clinical Chemistry/Central Laboratories, University and Medical Center Hamburg-Eppendorf, Martinistraße 52, 20246 Hamburg, Germany

ABSTRACT

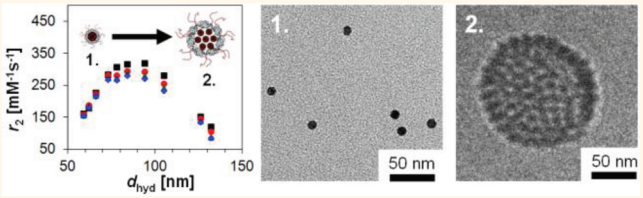

Concerning the outer sphere relaxation theory, the sensitivity of a T_2 MRI contrast agent, expressed by the transverse relaxivity r_2, depends on the diffusion length of water molecules relative to the particle size. For T_2-weighted spin–echo imaging, theoretical concepts reveal three regimes regarding the r_2 relaxivity depending on the nanocrystal size: the motional averaging regime (MAR), the static dephasing regime (SDR), and the echo-limiting regime (ELR). The r_2 maximum corresponds to the SDR, which represents a small size regime. To verify the theoretical concepts and to adjust the SDR, tailor-made T_2 contrast agents were synthesized by controlled self-assembly of superparamagnetic iron oxide nanocrystals (SPIOs) into raspberry-like nanoclusters with diameters of 30–200 nm using a PEG-based ligand. The results highlight an opportunity to optimize the relaxivity of T_2 contrast agents by tuning the cluster size of SPIO nanocrystals.

KEYWORDS: MRI · contrast agent · relaxivity · nanocrystal · SPIO · cluster

Superparamagnetic iron oxide (SPIO) nanocrystals are currently under intensive investigation as contrast agents for targeted *in vivo* imaging of cells and tissues by magnetic resonance imaging (MRI). In most of the cases, SPIOs are applied as so-called negative contrast agents. Hereby, the imaging contrast arises from shortening the transverse relaxation time T_2 of protons by the inhomogeneous magnetic field around the nanocrystals (outer sphere region) and leads to a darkening in the reconstructed image. In clinical MRI, one further distinguishes between T_2*- and T_2-weighted images, which are generated by gradient echo and spin–echo sequences, respectively. Whereas T_2 is the true transverse relaxation time, which is only determined by magnetic field fluctuations originating from the sample itself (SPIOs and differences in the chemical composition of the respective tissue or cell), T_2* also includes the contribution of the inhomogeneity of the external field.

The most challenging application of SPIOs is the targeted specific imaging of cells and tissues with sensitivity down to the single cell level. For this relaxation time, shortening by SPIOs should be highly effective, expressed by large values of the relaxivity r_2 (and r_2*), which is defined as

$$1/T_2 = 1/T_{2,0} + r_2 c_{Fe} \quad (1)$$

Herein $1/T_{2,0}$ is the reverse relaxation time of protons in the absence of SPIOs, and c_{Fe} is the analytical iron concentration. Large relaxivities are directly related to a large magnetization of the nanocrystals and thereby to their size.[1−4] This was experimentally proven for individually encapsulated iron oxide and manganese ferrite nanocrystals with sizes up to approximately 20 nm (often called ultrasmall SPIOs, USPIOs).[5] Maximum relaxivity for magnetite, however, is expected only at a particle size of 25 nm and for maghemite 27 nm[6] and could, therefore, not be achieved in these experiments. Unfortunately, no synthetic route for high-quality particles substantially larger than 20 nm is known so far. A way out of this dilemma is the clustering of small SPIOs to larger clusters. Indeed, clinically used contrast agents, such as resovist or endorem, exhibit a high degree of particle aggregation and therefore high relaxivities (typically

* Address correspondence to weller@chemie.uni-hamburg.de, elmar.poeselt@chemie.uni-hamburg.de.

Received for review November 25, 2011 and accepted January 25, 2012.

Published online January 25, 2012
10.1021/nn204591r

© 2012 American Chemical Society

between 150 and 200 mM^{-1} s^{-1}), and even better r_2* values of up to about 500 mM^{-1} s^{-1} were reported for SPIO aggregates encapsulated in liposomes.[7−9] Unfortunately, all the hitherto reported SPIO clustering approaches do not allow a precise control of the aggregate size. On the other hand, recent theoretical descriptions include size and clustering effects and lead to an empirical formula that allows an easy comparison with experimental results and mark the way to an optimized contrast agent.[10] In this paper, we present, for the first time, detailed experimental data on contrast optimization by controlled aggregation of SPIOs into stable and biocompatible clusters with narrow size distributions. We also show how the size of the originally prepared SPIOs influences the relaxivity of the final clusters and present a clear prove of the theoretically predicted complex size dependence of r_2.

RESULTS AND DISCUSSION

Recently, our group developed a micelle-forming triblock copolymer which allows the adjustment of the final micelle size and cluster rate of SPIO nanocrystals by varying the ratio of nanocrystals to polymer employed in the encapsulation process.[11] We adopted this method for the encapsulation and controlled clustering of SPIO nanocrystals with diameters of 4.0, 7.5, 8.7, 9.8, 11.8, and 13.1 nm, which were synthesized according to Hyeon *et al.*[12] These nanocrystals consist of γ-Fe_2O_3 (maghemite). However, Fe_3O_4 (magnetite), showing a higher saturation magnetization and density, is generally present together with γ-Fe_2O_3 after synthesis. Still, all calculations were made based on γ-Fe_2O_3. The triblock polymer used consisted of a branched poly(ethylene imine) (PEI) block with a molecular weight (M_W) of ≈700 g/mol, coupled to, on average, two to three poly-(ε-caprolactone)-*block*-poly(ethylene glycol) (PCL-*b*-PEG) chains. The average M_W of the PCL was 900 g/mol and of PEG 2000 g/mol. On average, 8−10 primary and secondary amines of the PEI block support the clustering of the nanocrystals in the interior of the PEI-*b*-PCL-*b*-PEG micelle by dative binding to the nanocrystal surface. A picture of PEI-*b*-PCL-*b*-PEG stabilized SPIO particles in water with different degrees of dilution is shown in the Supporting Information Figure S1.

To demonstrate the biological applicability of this polymer, a dilution series of PEI-*b*-PCL-*b*-PEG coated SPIO nanoparticles in ddH_2O, 3% BSA in PBS, pH 7.4, and pooled human blood plasma (BP), containing heparin and EDTA to inhibit coagulation, were prepared 24 h before the relaxivity measurement was performed at 37 °C (physiological temperature) to ensure that the system has regained its adsorption equilibrium. The relaxivity of the SPIO nanoparticles was measured at 1.41 T (60 MHz). In ddH_2O, a r_2 of 256 mM^{-1} s^{-1}, in BSA of 259 mM^{-1} s^{-1}, and in BP of 289 mM^{-1} s^{-1} (Supporting Information Figure S2) was

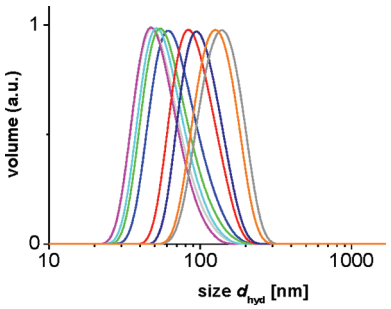

Figure 1. DLS volume distributions of PEI-*b*-PCL-*b*-PEG micelles containing 9.8 nm SPIO crystals. The average hydrodynamic diameter could be adjusted between 51 and 141 nm.

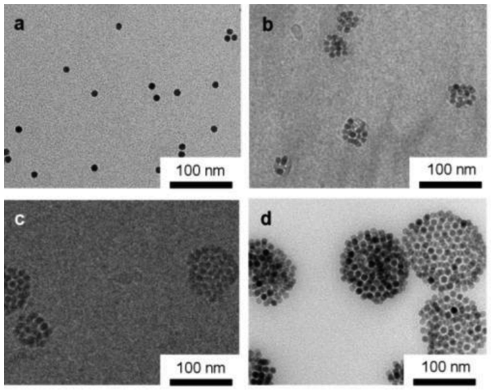

Figure 2. TEM image (a,d) and cryo-TEM images (b,c) of single and clustered 9.8 nm SPIOs. The d_{hyd} values, determined by DLS measurements, were 51 nm (a), 70 nm (b), 79 nm (c), and 141 nm (d).

measured. The very low increase in r_2 documents the high minimization of unspecific interactions. For more detailed information concerning, for example, stability in buffer solutions and against dilution, see ref 11.

Dynamic light scattering (DLS) measurements were performed to determine the hydrodynamic diameter (d_{hyd}) of the nanocomposites in water. Volume distributions for a series of different sized micelles containing 9.8 nm SPIO nanocrystals are shown exemplarily in Figure 1.

The corresponding transmission electron micrographs (TEM and cryo-TEM) of single and clustered 9.8 nm SPIO nanocrystals are shown with increasing degree of clustering in Figure 2a−d. As judged from the interparticle distance of Figure 2a, most nanocrystals of this sample are individually encapsulated, whereas in a few cases, also 2 or 3 SPIOs can be seen within the micelle core. As expected, TEM sizes are always somewhat smaller than the corresponding DLS values, whereby the largest deviation is observed for the individually encapsulated samples. It should be mentioned, however, that reliable TEM size histograms of the clustered samples can hardly be derived from the images, although we tested various preparation techniques and examined a large series of images. This is due to the fact that the clusters tend to collapse during drying or freezing.

T_2 relaxivity measurements of the nanocomposites were performed at 1.41 T at 37 °C with a pulse spacing, τ_{CP}, ranging from 0.05 to 1 ms. The transverse relaxivities, r_2, were determined by plotting the inverse relaxation time, which is the relaxation rate ($R_2 = 1/T_2$) against the analytical iron concentration, measured *via* flame atomic absorption spectrometry after nitric acid digestion (70 °C).

The r_2 dependence of the clustered SPIO micelles as a function of their volume weighted mean DLS size is shown in Figure 3. The results for clusters formed from 4.0 nm (a), 7.5 nm (b), 8.7 nm (c), 9.8 nm (d), 11.8 nm (e), and 13.1 nm (f) SPIOs are shown.

The plotted curves were calculated according to the theoretical studies of Gillis *et al.*[10] and will be discussed further below. Except for the 4 nm nanocrystals (Figure 3a), all graphs show three different size regimes of r_2 with increasing cluster diameter: an increase in the so-called motional average regime (MAR), a maximum in the static dephasing regime (SDR), and an echo-dependent decrease of r_2 in the echo-limiting regime (ELR)[6,13] (schematically shown in Figure 4a).

In our measurements, a dependency of r_2 on the size of the nanocrystals was observed. With increasing nanocrystal size, an increase of r_2 in the SDR was determined. The r_2 relaxivity in the SDR (τ_{CP} = 1 ms) is linearly dependent on the volume of the differently sized, single SPIO nanocrystals (V_{SPIO}) in Figure 5. Thus, corresponding to Carroll *et al.*,[1] the maximum of r_2 of 4 nm SPIOs is expected to be higher than we could achieve by clustering in our size regime.

In general, the size dependence of the transverse relaxivity originates from the diffusion length of water molecules relative to the size of the magnetic particle. This is expressed by the diffusion time, τ_D, which is defined by the particle diameter, d, and the water diffusion coefficient, D, *via* eq 2.

$$\tau_D = d^2/4D \qquad (2)$$

We will now briefly discuss these regimes following the calculations of Gillis *et al.*[10] for compact magnetic spheres and will then compare the results with our experimentally observed values.

As long as $\tau_D < 1/(\gamma B_{eq})$, the MAR condition is fulfilled (γ is the proton gyromagnetic ratio and B_{eq} is the equatorial magnetic field of the SPIO).[13] Due to their diffusion, the protons experience changing magnetic fields, which are effectively time-averaged.[1] In the MAR, the relaxation rate, R_2 (and also R_2*) is given by the quantum mechanical outer sphere theory under negligence of the self-relaxation of water, $T_{2,O}$ ($R_2 = 1/T_2 - 1/T_{2,O}$):

$$R_2 = (16/45)\nu\tau_D(\gamma B_{eq})^2 \qquad (3)$$

where ν is the volume fraction occupied by the magnetized spheres.[6,10,14] R_2 and consequently r_2 increases with increasing size of the nanocrystal cluster and is independent of the echo time.

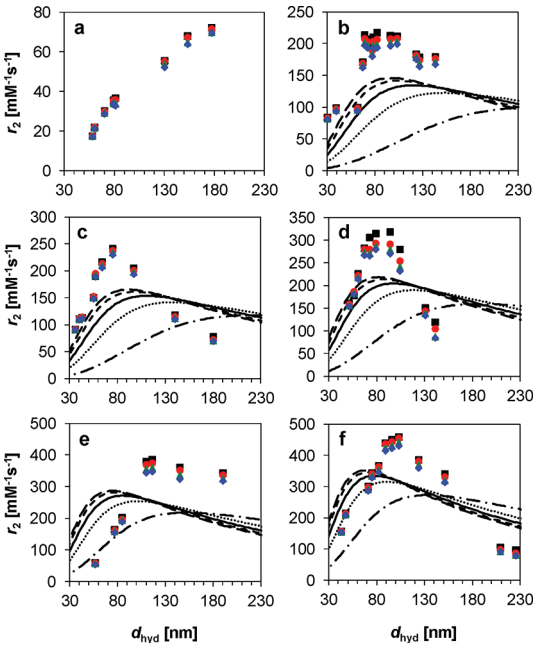

Figure 3. The r_2 relaxivity of SPIO-containing PEI-*b*-PCL-*b*-PEG micelles with respect to the hydrodynamic diameter d_{hyd} obtained from the volume distribution measured by DLS. The measurements were performed at 1.41 T with pulse spacings, τ_{CP}, of 1 ms (black square), 0.3 ms (red circle), 0.1 ms (green triangle), and 0.05 ms (blue diamond). The applied SPIO crystals had a diameter of 4.0 nm (a), 7.5 nm (b), 8.7 nm (c), 9.8 nm (d), 11.8 nm (e), and 13.1 nm (f). For the large clusters of SPIO crystals with a higher saturation magnetization, the SDR could be reached and the typical echo time dependence could be observed with decreasing relaxivity for the shorter echo times. The black lines are fitted using the formula given by Gillis *et al.*[10] (eq 7). The organic layer of the SPIO nanocrystals was calculated with 0.25 nm (– – –), 0.5 nm (- - -), 1 nm (—), 2 nm (· · ·), and 5 nm (– · – · –).

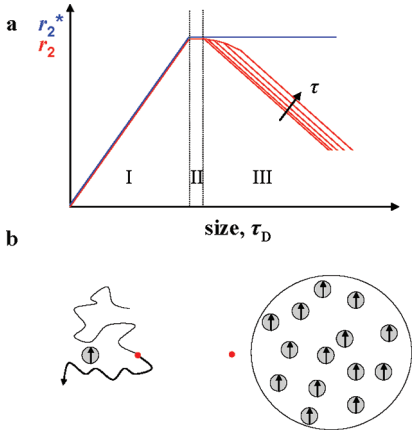

Figure 4. Schematic illustration of the relaxivity dependence on cluster size as predicted by the outer sphere relaxation theory. (a) Dependence of r_2 and r_2* on cluster size in MAR (I), SDR (II), and ELR (III). (b) In the MAR, a water molecule (red dot) experiences different magnetic fields during relaxation due to its diffusion (left), whereas the field fluctuations are negligible in the SDR.

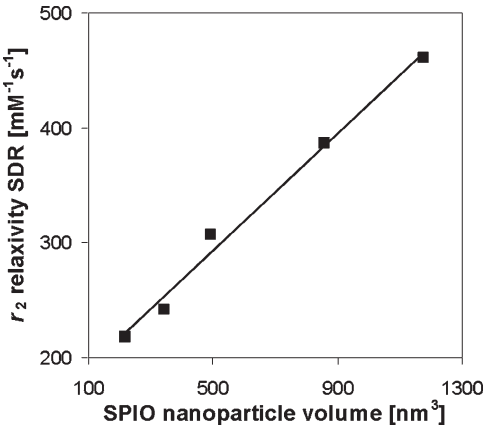

Figure 5. Dependency of the r_2 relaxivity maxima (SDR) of clustered SPIO nanocrystals on the volume of the SPIO nanocrystals (diameters: 7.5, 8.7, 9.8, 11.8, and 13.1 nm) at a τ_{CP} of 1 ms.

The equatorial magnetic field B_{eq} of the crystal is related to the magnetization of the particle by[6,10]

$$B_{eq} = \frac{\mu_0}{3} M \quad (4)$$

with μ_0 as the magnetic constant, ($\mu_o = 4\pi \times 10^{-4} T/(\text{emu/cm}^3)$), and M the crystal, that is, cluster, magnetization. M of the crystals depends on the crystal size. Due to the reduced spin−spin exchange coupling energy at the surface, the nanocrystals possess a magnetically disordered spin glass-like layers near the surface.[15,16] These surface canting effects become more dominant for smaller crystals due to the increased surface to volume ratio. This leads to a reduction in the saturation magnetization value.[17]

At a certain particular size or clustering rate, R_2 or rather r_2 no longer increases with increasing cluster size (region II in Figure 4). The particle size is so large that water molecules feel a constant magnetic field during their relaxation. Here, the SDR is reached, which places an absolute limit to the relaxivities, which are given by eq 5[6,10]

$$R^*_2 = \frac{2\pi}{3\sqrt{3}} \nu\gamma B_{eq} \quad (5)$$

Since in the SDR, R_2 and R_2* are equal, eq 5 can be transformed into an r_2 dependency ($R_2 = r_2 \times c_{Fe}$) on introducing a conversion factor a to transform the Fe concentration ($\nu = a \times c_{Fe}$; for further details, see Supporting Information).

$$r_2 = \frac{2\pi}{3a\sqrt{3}} \gamma B_{eq} \quad (6)$$

Thus, B_{eq} can be obtained from the maximum relaxivity (cf. also Figure 5). Subsequently, at larger d values, a decrease in r_2 occurs, whereas r_2* remains constant (ELR, region III in Figure 4). The decrease depends on the echo time τ_{CP}, which is the time interval between a 180° refocusing pulse and the subsequent echo maximum in a typical T_2-weighted spin−echo sequence. The longer the time between the refocusing pulses, the longer is the echo time and the refocusing pulse can rephase the fewer spins. This shortens T_2 and increases r_2.

In ref 10, the authors give an empirical expression, which fits their Monte Carlo simulations in a very good manner, which we converted into r_2:

$$r_2 = a \frac{(jB_{eq} \cdot d/2)^2}{1 + kd/2B^{\alpha}_{eq} + (ld/2B^{\alpha}_{eq})^2 + (pd/2B^{\alpha}_{eq})^3 + (qd/2B^{\alpha}_{eq})^4} \quad (7)$$

with $\alpha = 0.42$, $j = 2.5209 \times 10^{12}$, $k = -0.1177 \times 10^9$, d the particle diameter, $l = 0.1295 \times 10^9$, $p = 0.0523 \times 10^9$, $q = 0.0566 \times 10^9$. We used eq 7 with the experimentally determined B_{eq} values to fit our experimental data in Figure 3. Thus, we treated our clusters as solid magnetic spheres. This assumption is allowed because the interspaces between the individual nanocrystals within the clusters are filled with surface-bound oleic acid ligands. Such a structure can be considered as a dilute maghemite phase through which no water molecules can defuse. We take this into account by assuming a 0.25, 0.5, 1, 2, and 5 nm thick shell of oleic acid around the particles and correcting the density of clusters formed by the respective original nanocrystal size (for details of this correction, see the Supporting Information). The fit shows that the density of the SPIO crystals inside of the particle influences the overall magnetization of the particle. Thus, with increasing amount of organic, the overall magnetization of the particle decreases. This results in a lower maximum relaxivity in SDR and a shift of the SDR to higher cluster diameter.

The comparison of the calculated and the measured curves is only moderately satisfactory, whereby best fits are obtained for inter particle distances of 1 nm or below. Such small values are in accordance to the SEM images and result from the encapsulation procedure, in which a large fraction of oleic acid ligands are removed. Deviation of the fitted curves from the experimental data may have various reasons. First of all, we used the hydrodynamic diameter of the encapsulated clusters, which also includes the ligand shell and the solvation sphere. As outlined above, this is the only feasible way since a reliable determination of the exact cluster diameter by TEM was impossible. Especially for the small clusters, the deviation should be relatively large. With this argument, it might be reasonable to shift the fitted curve horizontally by 20−30 nm, which is the expected shell thickness. This would improve the agreement substantially, but we would like to leave this to the reader. A further crucial point is the assumption of the volume fraction of iron oxide within the cluster since the exact amount of oleic acid is not known and might vary due to the transfer of the

TABLE 1. Calculated Values of the Cluster Density ρ_{CL} Neglecting the Outer Polymer Shell and the Cluster Magnetization M_{CL} Calculated by Equations 4 and *6*

d_{SPIO} [nm]	ρ_{CL} [g/cm^3]	M_{CL} [emu/cm^3]
4.0	2.1	
7.5	2.9	49
8.7	3.0	59
9.8	3.2	80
11.8	3.4	110
13.1	3.5	137

hydrophobic SPIOs into the micelle core during the encapsulation and phase transfer to water. Another reason might be the theoretical approach itself. Gillis *et al.* argued in a recent paper that the theory should only give semiquantitative agreement with experimental data. Finally, the theory assumes that the water molecules can diffuse to the surface of the magnetic core and therefore feel the equatorial field. In our case, however, a tightly bound ligand shell surrounds the core with a hydrophobic moiety followed by the PEG region with reduced water diffusivity. Thus, these protons always experience SDR conditions. We expect that this also modifies the size-dependent relaxivity in the MAR. Taking all of these considerations into account, the agreement between theory and experiment is reasonable.

Equations 4 and 6 allow the calculation of the cluster magnetization in the SDR. The corresponding values are listed in Table 1.

The values ranging from 49 to 137 emu/cm^3 are significantly lower than the magnetization of bulk material (420 emu/cm^3). Even if we subtract the contribution of oleic acid, the values are still lower than reported for the size-dependent magnetization of maghemite.[1,10] This might be an intrinsic problem arising from the above-mentioned complications in applying the theoretical model to our encapsulated clusters. It shows, however, that the relaxivities might be further increased by using larger nanocrystals and less oleic acid ligands during clustering.

CONCLUSION

In summary, we were able to tune the r_2 relaxivity of PEI-*b*-PCL-*b*-PEG stabilized SPIO nanocrystals by controlled clustering. We identified points of action for relaxivity optimization and were able to synthesize optimized contrast agents for the given SPIO crystal sizes. Herein, it was demonstrated that, with increasing number of nanocrystals, the relaxivity follows the computer simulations of Gillis *et al.*[10] With increasing size, the motional averaging regime (MAR), the static dephasing regime (SDR), and the echo-limiting regime (ELR) were observed. The relaxivity in the SDR depends on the magnetic properties of the clusters. Consequently, to form an r_2-optimized contrast agent for T_2-weighted spin−echo imaging, the number of clustered crystals has to be adjusted to the size of the maximum relaxivity r_2 given by the SDR. The magnetization of the nanocrystals should be as close as possible to that of bulk material. In addition, the fraction of the SPIO nanocrystals in the particle should be high to achieve a high overall magnetization of the composite. In our experiments, the highest relaxivities were obtained by clustered 13.1 nm particles. Smaller crystals with a reduced saturation magnetization exhibit lower r_2 maxima. The smallest used SPIO crystals of 4 nm in size showed no SDR in our measurement range (d_{hyd}) due to their weak magnetic properties. Furthermore, the particle size could effect in *in vivo* applications, for example, the blood circulation time and the enhanced permeability and retention (EPR) effect in tumor targeting. The here presented method allows an independent control over particle size and relaxivity.

METHODS

Nanocrystal Synthesis. SPIO nanocrystals were synthesized according to Hyeon *et al.*[12] The nanocrystals were purified by precipitation with ethanol. After dissolving in chloroform the nanocrystals were two-fold precipitated with acetone. The nanocrystals were stored in chloroform.

Phase Transfer. The phase transfer was done according to our previous publication.[11] The nanocrystals were precipitated with acetone. After being dried, the nanoparticles were dissolved in THF and the PEI-*b*-PCL-*b*-PEG polymer was added in a 5−1000-fold molar excess. After 10 min, water was added, and THF was removed in nitrogen flow. The final iron concentration was determined by flame atomic absorption spectrometry (PE 5000 spectrometer, Perkin-Elmer). Therefore, the SPIO nanocrystals were dissolved in 32.5% nitric acid (suprapur) for 2 h at 75 °C.

Relaxivity Measurements. Relaxometric measurements were performed at a Minispec mq60 (1.41 T) from Bruker Optics (Ettlingen, Germany) at 37 °C.

DLS. Dynamic light scattering (DLS) measurements were carried out with a Malvern Zetasizer Nano ZS system.

TEM. Transmission electron microscope measurements were performed with a JEOL JEM-1011 microscope. For Cryo-TEM images, a Tecnai G2 Spirit 120 transmission electron microscope was used.

Conflict of Interest: The authors declare no competing financial interest.

Acknowledgment. The authors would like to thank Mrs. Torborg Krugmann of the research group of Prof. J.A.C. Broekaert of the Chemistry Department of the University of Hamburg for performing numerous iron concentration determinations by flame atomic absorption spectrometry. We also thank Sunhild Salmen from the rtesearch group of Prof. H. Weller for the synthesis of the 7.5 and 13.1 nm SPIO crystals, and Ulf König for recording the cryo-TEM images. This work was supported by the European Union's Seventh Framework Programme (VIBRANT, FP7-228933-2).

Supporting Information Available: Calculations of factor a, a picture of the particle solutions, stability tests, and complete refs 3 and 7. This material is available free of charge *via* the Internet at http://pubs.acs.org.

REFERENCES AND NOTES

1. Carroll, M. R. J.; Woodward, R. C.; House, M. J.; Teoh, W. Y.; Amal, R.; Hanley, T. L.; St Pierre, T. G. Experimental Validation of Proton Transverse Relaxivity Models for Superparamagnetic Nanoparticle MRI Contrast Agents. *Nanotechnology* **2010**, *21*, 035103.
2. Park, Y. I.; Piao, Y.; Lee, N.; Yoo, B.; Kim, B. H.; Choi, S. H.; Hyeon, T. Transformation of Hydrophobic Iron Oxide Nanoparticles to Hydrophilic and Biocompatible Maghemite Nanocrystals for Use as Highly Efficient MRI Contrast Agent. *J. Mater. Chem.* **2011**, *21*, 11472–11477.
3. Tromsdorf, U. I.; Bigall, N. C.; Kaul, M. G.; Bruns, O. T.; Nikolic, M. S.; Mollwitz, B.; Sperling, R. A.; Reimer, R; Hohenberg, H.; Parak; *et al.* Size and Surface Effects on the MRI Relaxivity of Manganese Ferrite Nanoparticle Contrast Agents. *Nano Lett.* **2007**, *7*, 2422–2427.
4. Figuerola, A.; Di Corato, R.; Manna, L.; Pellegrino, T. From Iron Oxide Nanoparticles towards Advanced Iron-Based Inorganic Materials Designed for Biomedical Applications. *Pharmacol. Res.* **2010**, *62*, 126–143.
5. Mornet, S.; Vasseur, S.; Grasset, F.; Duguet, E. Magnetic Nanoparticle Design for Medical Diagnosis and Therapy. *J. Mater. Chem.* **2004**, *14*, 2161–2175.
6. Gillis, P.; Moiny, F.; Brooks, A. R. On T_2-Shortening by Strongly Magnetized Spheres: A Partial Refocusing Model. *Magn. Reson. Med.* **2002**, *47*, 257–263.
7. Bruns, O. T; Ittrich, H.; Peldschus, K.; Kaul, M. G.; Tromsdorf, U. I.; Lauterwasser, J.; Nikolic, M. S.; Mollwitz, B.; Merkel, M.; Bigall, N. C.; *et al.* Real-Time Magnetic Resonance Imaging and Quantification of Lipoprotein Metabolism *in Vivo* Using Nanocrystals. *Nat. Nanotechnol.* **2009**, *4*, 193–201.
8. Soenen, S. J.; Vande Velde, G.; Ketkar-Atre, A.; Himmelreich, U.; De Cuyper, M. Magnetoliposomes as Magnetic Resonance Imaging Contrast Agents. *Adv. Rev.* **2011**, *3*, 197–211.
9. Bogdanov, A. A., Jr.; Martin, C.; Weissleder, R.; Brady, T. J. Trapping of Dextran Coated Colloids in Liposomes by Transient Binding to Aminophospholipid: Preparation of Ferrosomes. *Biochim. Biophys. Acta* **1994**, *1193*, 212–218.
10. Vuong, Q. L.; Gillis, P.; Gossuin, Y. Monte Carlo Simulation and Theory of Proton NMR Transverse Relaxation Induced by Aggregation of Magnetic Particles Used as MRI Contrast Agents. *J. Magn. Reson.* **2011**, *212*, 139–148.
11. Pöselt, E.; Fischer, S.; Förster, S.; Weller, H. Highly Stable Biocompatible Inorganic Nanoparticles by Self-Assembly of Triblock-Copolymer Ligands. *Langmuir* **2009**, *25*, 13906–13913.
12. Hyeon, T.; Lee, S. S.; Park, J.; Chung, Y.; Na, H. B. Synthesis of Highly Crystalline and Monodisperse Maghemite Nanocrystallites without a Size-Selection Process. *J. Am. Chem. Soc.* **2001**, *123*, 12798–12801.
13. Brooks, R. A. T_2-Shortening by Strongly Magnetized Spheres: A Chemical Exchange Model. *Magn. Reson. Med.* **2002**, *47*, 388–391.
14. Roch, A.; Gossuin, Y.; Muller, R. N.; Gillis, P. Superparamagnetic Colloid Suspensions: Water Magnetic Relaxation and Clustering. *J. Magn. Magn. Mater.* **2005**, *293*, 532–539.
15. Morales, M. P.; Veintemillas-Verdaguer, S.; Montero, M. I.; Serna, C. J.; Roig, A.; Casas, L.; Martinez, B.; Sandiumenge, F. Surface and Internal Spin Canting in γ-Fe_2O_3 Nanoparticles. *Chem. Mater.* **1999**, *11*, 3058–3064.
16. Morales, M. P.; Serna, C. J.; Bodker, F.; Morup, S. Spin Canting Due to Structural Disorder in Maghemite. *J. Phys.: Condens. Matter* **1997**, *9*, 5461–5467.
17. Jun, Y.-W.; Seo, J.-W.; Cheon, J. Nanoscaling Laws of Magnetic Nanoparticles and Their Applicabilities in Biomedical Sciences. *Acc. Chem. Res.* **2008**, *41*, 179–189.